5G-Aided RTK Positioning in GNSS-Deprived Environments

Pinjun Zheng, Xing Liu, Tarig Ballal, Tareq Y. Al-Naffouri
Computer, Electrical and Mathematical Science & Engineering
King Abdullah University of Science and Technology (KAUST), Thuwal, KSA
Email: {pinjun.zheng; xing.liu; tarig.ahmed; tareq.alnaffouri}@kaust.edu.sa

***Abstract*—This paper considers the localization problem in a 5G-aided global navigation satellite system (GNSS) based on real-time kinematic (RTK) technique. Specifically, the user's position is estimated based on the hybrid measurements, including GNSS pseudo-ranges, GNSS carrier phases, 5G angle-of-departures, and 5G channel delays. The underlying estimation problem is solved by steps that comprise obtaining the float solution, ambiguity resolution, and resolving the fixed solution. The analysis results show that the involvement of 5G observations can enable localization under satellite-deprived environments, inclusive of extreme cases with only 2 or 3 visible satellites. Moreover, extensive simulation results reveal that with the help of 5G observations, the proposed algorithm can significantly reduce the estimation error of the user's position and increase the success rate of carrier-phase ambiguity resolution.**

***Index Terms*—GNSS, 5G/6G, localization, RTK, ambiguity resolution.**

I. Introduction

Accurate localization has become an essential requirement for a broad variety of applications, such as intelligent transportation, precision agriculture, surveying and mapping, and smart cities [1]–[3]. The development of advanced unmanned systems in recent years motivates a further increase in the demand for high positioning accuracy and reliability [4], [5]. Although plenty of navigation techniques have been developed for outdoor positioning, global navigation satellite system (GNSS)-based positioning is the most prevalent thanks to its advantages of high accuracy, global coverage, low cost, and all-weather capability.

Real-time kinematic (RTK) is a widely-used GNSS-based positioning technique. In RTK positioning, a GNSS base station (BS) installed at a fixed position and the user's GNSS receiver collect GNSS observations simultaneously. The BS transmits its observation (the pseudo-range and carrier-phase) together with its accurate position to the user via a suitable communication link [6]. The involvement of GNSS carrier-phase observations, differential correction, and ambiguity resolution enables RTK positioning to provide centimeter-level accuracy in open-sky scenarios [7], [8]. However, the performance of RTK in deep urban environments is not up to par with the high-accuracy requirements for many dynamic systems. In such environments, buildings can block, weaken, reflect, and diffract the GNSS signals, which may result in an insufficient number of visible satellites and observations with severe multipath effects [9]. Providing reliable navigation in these situations is a daunting task that is yet to be accomplished.

To address the limitations of RTK positioning, fusing various sensor types (including inertial navigation systems, optical sensors, Lidar, etc.) with GNSS has been explored [10], [11]. Recently, with the emergence of the fifth generation (5G) wireless systems which are expected to provide high-precision localization services, many promising results about 5G localization have been reported in the literature [12]–[15]. To take advantage of these emerging technologies, GNSS augmentation with 5G has been considered. Examples of such works include hybrid GNSS-5G positioning based on device-to-device measurements [16], neural network fingerprinting and GNSS data fusion [17], multi-rate 5G and GNSS data fusion [18], and a few more [19], [20].

This paper utilizes 5G observations to aid RTK positioning to overcome its shortcomings in GNSS-deprived environments. Our main contribution is proposing a method to leverage 5G observations in GNSS carrier-phase ambiguity resolution, especially in harsh environments with poor satellite visibility. We formulate the localization problem by jointly using GNSS and 5G observations. The problem is solved through three steps, namely, computing a float solution, ambiguity resolution, and computing the fixed solution. In addition, we perform a localization availability analysis which demonstrates that the introduction of the 5G observations can enable localization in extreme scenarios with only 2 or 3 visible satellites.

II. System Model

We consider a 5G-aided RTK positioning system with N visible satellites, a user equipment with an unknown position, a GNSS BS with a known position, and L 5G BSs with known positions and orientations. A 5G radio link is established between the GNSS BS and the user. The user can receive both GNSS and 5G signals. An example of the considered system with $N = 3$ and $L = 1$ is illustrated in Fig. 1. For clarity, we use superscripts $(\cdot)^n$ to denote the variables related to the n-th satellite, subscripts $(\cdot)_u$, $(\cdot)_b$ and $(\cdot)_{\mathrm{B}}$ represent the variables related to the user, the GNSS BS and the 5G BS, respectively. We denote the user position as $\mathbf{p}_u \in \mathbb{R}^3$ and the position of the GNSS BS as $\mathbf{p}_b \in \mathbb{R}^3$. The position and orientation of the ℓ-th 5G BS are denoted as $\mathbf{p}_{\mathrm{B},\ell} \in \mathbb{R}^3$ and $\mathbf{R}_{\mathrm{B},\ell} \in \mathrm{SO}(3)$, respectively. Here SO(3) denotes the special

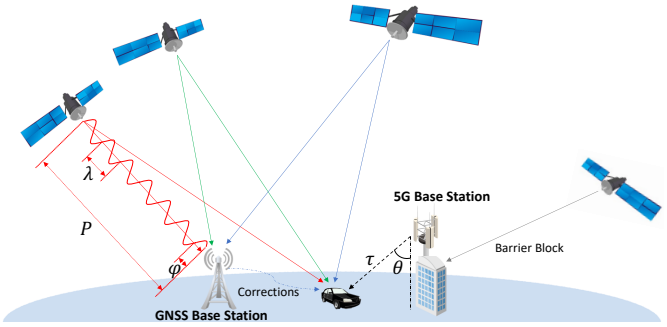

Fig. 1. Illustration of a 5G-aided RTK positioning system with three satellites and one 5G BS.

orthogonal group of three-dimensional (3D) rotation matrices $\mathrm{SO}(3) = \{\mathbf{R}|\mathbf{R}^\mathsf{T}\mathbf{R} = \mathbf{I}_3, \det(\mathbf{R}) = 1\}$.

A. RTK Model

The main GNSS observations from the n-th satellite received by the user are the pseudo-range P_u^n and carrier-phase ϕ_u^n. These observations are often modeled as

$$P_u^n = \rho_u^n + I_u^n + T_u^n + c\,(\delta t_u - \delta t^n) + \varepsilon_u^n, \tag{1}$$
$$\varphi_u^n = \rho_u^n + \lambda K_u^n - I_u^n + T_u^n + c\,(\delta t_u - \delta t^n) + \varsigma_u^n, \tag{2}$$

where ρ denotes the geometrical range between the GNSS receiver and the satellite, λ represents the wavelength of the GNSS carrier, K represents the carrier-phase ambiguity, I is the ionospheric delay, T is the tropospheric delay, δt is the receiver or satellite clock bias, and ε and ς lump errors from other sources together with additive noise.

RTK positioning takes advantage of differencing operations to virtually cancel common errors between the GNSS receivers and satellites. First, the user's and the GNSS BS's measurements collected simultaneously are differenced to eliminate the satellite clock bias and atmospheric delays, resulting in the *single-difference* (SD) model [21]:

$$P_{ub}^n = P_u^n - P_b^n = \rho_{ub}^n + c\delta t_{ub} + \varepsilon_{ub}^n,$$
$$\varphi_{ub}^n = \varphi_u^n - \varphi_b^n = \rho_{ub}^n + \lambda K_{ub}^n + c\delta t_{ub} + \varsigma_{ub}^n.$$

Defining the unit direction vector of the satellite-user line-of-sight (LOS) as $\mathbf{h}_u^n$, we can obtain the following relationship based on the far-field assumption:

$$\rho_{ub}^n = \rho_u^n - \rho_b^n = (\mathbf{h}_u^n)^\mathsf{T}(\mathbf{p}_u - \mathbf{p}_b). \tag{3}$$

Subsequently, the SD observations are again differenced over pairs of satellites to remove the receiver clock bias, which yields the *double-difference* (DD) model:

$$P_{ub}^{nm} = P_{ub}^n - P_{ub}^m = (\mathbf{h}_u^n - \mathbf{h}_u^m)^\mathsf{T}(\mathbf{p}_u - \mathbf{p}_b) + \varepsilon_{ub}^{nm},$$
$$\varphi_{ub}^{nm} = \varphi_{ub}^n - \varphi_{ub}^m = (\mathbf{h}_u^n - \mathbf{h}_u^m)^\mathsf{T}(\mathbf{p}_u - \mathbf{p}_b) + \lambda K_{ub}^{nm} + \varsigma_{ub}^{nm}.$$

Without loss of generality, we take the 1-st satellite as a reference and concatenate all the DD observations as

$$\mathbf{p} = [P_{ub}^{21}, P_{ub}^{31}, \ldots, P_{ub}^{N1}]^\mathsf{T} \in \mathbb{R}^{N-1}, \tag{4}$$
$$\boldsymbol{\phi} = [\varphi_{ub}^{21}, \varphi_{ub}^{31}, \ldots, \varphi_{ub}^{N1}]^\mathsf{T} \in \mathbb{R}^{N-1}. \tag{5}$$

The noise-free observation model of the RTK can be summarized as

$$\mathbf{y}_1 = \begin{bmatrix}\mathbf{p}\\ \boldsymbol{\phi}\end{bmatrix} = \underbrace{\begin{bmatrix}\mathbf{H}\\ \mathbf{H}\end{bmatrix}}_{\mathbf{B}}\mathbf{p}_u + \underbrace{\begin{bmatrix}\mathbf{0}\\ \lambda\mathbf{I}\end{bmatrix}}_{\mathbf{C}}\mathbf{k} - \underbrace{\begin{bmatrix}\mathbf{H}\\ \mathbf{H}\end{bmatrix}}_{\mathbf{b}}\mathbf{p}_b \in \mathbb{R}^{2N-2}, \tag{6}$$

where

$$\mathbf{H} = \left[(\mathbf{h}_u^2 - \mathbf{h}_u^1), \ldots, (\mathbf{h}_u^N - \mathbf{h}_u^1)\right]^\mathsf{T} \in \mathbb{R}^{(N-1)\times 3},$$
$$\mathbf{k} = \left[K_{ub}^{21}, K_{ub}^{31}, \ldots, K_{ub}^{N1}\right]^\mathsf{T} \in \mathbb{R}^{N-1}.$$

B. 5G Model

Besides the GNSS measurements, the user can receive 5G signals from L BSs. For simplicity, we assume that an *efficient* channel estimator is applied and the angle-of-departures (AODs) $\{\boldsymbol{\theta}_\ell\}_{\ell=1}^L$ and channel delays $\{\tau_\ell\}_{\ell=1}^L$ are available as the 5G observations [14]. Note that each AOD $\boldsymbol{\theta}_\ell$ comprises an azimuth angle $\theta_\ell^{\mathrm{az}}$ and an elevation angle $\theta_\ell^{\mathrm{el}}$. The 5G observation model is given by

$$\theta_\ell^{\mathrm{az}} = \mathrm{atan2}\left([\mathbf{R}_{\mathrm{B},\ell}^\mathsf{T}(\mathbf{p}_u - \mathbf{p}_{\mathrm{B},\ell})]_2, [\mathbf{R}_{\mathrm{B},\ell}^\mathsf{T}(\mathbf{p}_u - \mathbf{p}_{\mathrm{B},\ell})]_1\right), \tag{7}$$
$$\theta_\ell^{\mathrm{el}} = \mathrm{asin}\left([\mathbf{R}_{\mathrm{B},\ell}^\mathsf{T}(\mathbf{p}_u - \mathbf{p}_{\mathrm{B},\ell})]_3 / \|\mathbf{p}_u - \mathbf{p}_{\mathrm{B},\ell}\|_2\right), \tag{8}$$
$$\tau_\ell = \frac{\|\mathbf{p}_{\mathrm{B},\ell} - \mathbf{p}_u\|_2}{c} + \Delta, \tag{9}$$

where $[\cdot]_i$ denotes the i-th entry of a vector, c is the speed of light, and Δ is the unknown clock bias between the 5G BS and the user. We further stack these 5G observations as $\boldsymbol{\theta}^{\mathrm{az}} = [\theta_1^{\mathrm{az}}, \theta_2^{\mathrm{az}}, \ldots, \theta_L^{\mathrm{az}}]^\mathsf{T}$, $\boldsymbol{\theta}^{\mathrm{el}} = [\theta_1^{\mathrm{el}}, \theta_2^{\mathrm{el}}, \ldots, \theta_L^{\mathrm{el}}]^\mathsf{T}$, $\boldsymbol{\tau} = [\tau_1, \tau_2, \ldots, \tau_L]^\mathsf{T}$, and finally in one vector as

$$\mathbf{y}_2 = [(\boldsymbol{\theta}^{\mathrm{az}})^\mathsf{T}, (\boldsymbol{\theta}^{\mathrm{el}})^\mathsf{T}, \boldsymbol{\tau}^\mathsf{T}]^\mathsf{T} \in \mathbb{R}^{3L}. \tag{10}$$

C. Problem Formulation

For a joint 5G-RTK localization formulation, suppose we have two noisy observation vectors $\hat{\mathbf{y}}_1$ and $\hat{\mathbf{y}}_2$, and the corresponding covariance matrices are available and denoted as $\mathbf{Q}_{\hat{\mathbf{y}}_1}$ and $\mathbf{Q}_{\hat{\mathbf{y}}_2}$. The unknown parameters are defined as

$$\mathbf{x} \triangleq [\mathbf{p}_u^\mathsf{T}, \mathbf{k}^\mathsf{T}, \Delta]^\mathsf{T} \in \mathbb{R}^{N+3}. \tag{11}$$

Based on the developed RTK model (6) and 5G model (7)–(9), we can construct the following optimization problem

$$\underset{\mathbf{p}_u\in\mathbb{R}^3, \mathbf{k}\in\mathbb{Z}^{N-1}, \Delta\in\mathbb{R}}{\arg\min} \quad \epsilon\|\hat{\mathbf{y}}_1 - \mathbf{A}\mathbf{x} + \mathbf{b}\|_{\mathbf{W}_1}^2 + (1-\epsilon)\|\hat{\mathbf{y}}_2 - \mathbf{y}_2(\mathbf{x})\|_{\mathbf{W}_2}^2, \tag{12}$$

where $\epsilon \in [0,1]$ is a weighting factor, and $\|(\cdot)\|_{\mathbf{W}}^2 \triangleq (\cdot)^\mathsf{T}\mathbf{W}(\cdot)$. The matrix $\mathbf{A}$ is defined as

$$\mathbf{A} \triangleq \begin{bmatrix}\mathbf{H} & \mathbf{0} & \mathbf{0}\\ \mathbf{H} & \lambda\mathbf{I} & \mathbf{0}\end{bmatrix} \in \mathbb{R}^{(2N-2)\times(N+3)}, \tag{13}$$

and the nonlinear function $\mathbf{y}_2(\mathbf{x})$ are represented by (7)–(9).

In this work, we use the weight matrices $\mathbf{W}_1$ and $\mathbf{W}_2$ as

$$\mathbf{W}_1 = \mathbf{Q}_{\hat{\mathbf{y}}_1}^{-1} / \|\mathbf{Q}_{\hat{\mathbf{y}}_1}^{-1}\|_{\mathrm{F}}, \quad \mathbf{W}_2 = \mathbf{Q}_{\hat{\mathbf{y}}_2}^{-1} / \|\mathbf{Q}_{\hat{\mathbf{y}}_1}^{-1}\|_{\mathrm{F}}, \tag{14}$$

where $\|\cdot\|_{\mathrm{F}}$ stands for the Frobenius norm.

III. Methodology

This section proposes a gradient-based solution for (12) and localization availability is discussed. To be clear, we start from the typical RTK routine with integer least-squares (ILS), based on which the proposed algorithm is developed.

A. ILS-based RTK Solution

According to the standalone RTK model (6), we have the following (mixed) ILS problem [21]:

$$\underset{\mathbf{p}_u\in\mathbb{R}^3,\mathbf{k}\in\mathbb{Z}^{N-1}}{\arg\min} \|\mathbf{y}_1-\mathbf{B}\mathbf{p}_u-\mathbf{C}\mathbf{k}+\mathbf{b}\|^2_{\mathbf{W}_1}. \tag{15}$$

It is not straightforward to solve (15) due to the presence of the integer constraint on $\mathbf{k}$. To simplify the problem, one can first ignore the constraint to obtain a *float* solution as a starting point to perform the integer search. Based on the least-squares (LS) estimation principle, the float solution reads

$$\begin{bmatrix}\hat{\mathbf{p}}_u\\ \hat{\mathbf{k}}\end{bmatrix}=\begin{bmatrix}\mathbf{B}^\mathsf{T}\mathbf{W}_1\mathbf{B} & \mathbf{B}^\mathsf{T}\mathbf{W}_1\mathbf{C}\\ \mathbf{C}^\mathsf{T}\mathbf{W}_1\mathbf{B} & \mathbf{C}^\mathsf{T}\mathbf{W}_1\mathbf{C}\end{bmatrix}^{-1}\begin{bmatrix}\mathbf{B}^\mathsf{T}\mathbf{W}_1(\mathbf{y}_1+\mathbf{b})\\ \mathbf{C}^\mathsf{T}\mathbf{W}_1(\mathbf{y}_1+\mathbf{b})\end{bmatrix}, \tag{16}$$

with the covariance matrix given by

$$\begin{bmatrix}\mathbf{Q}_{\hat{\mathbf{p}}_u} & \mathbf{Q}_{\hat{\mathbf{p}}_u\hat{\mathbf{k}}}\\ \mathbf{Q}_{\hat{\mathbf{k}}\hat{\mathbf{p}}_u} & \mathbf{Q}_{\hat{\mathbf{k}}}\end{bmatrix}=\begin{bmatrix}\mathbf{B}^\mathsf{T}\mathbf{W}_1\mathbf{B} & \mathbf{B}^\mathsf{T}\mathbf{W}_1\mathbf{C}\\ \mathbf{C}^\mathsf{T}\mathbf{W}_1\mathbf{B} & \mathbf{C}^\mathsf{T}\mathbf{W}_1\mathbf{C}\end{bmatrix}^{-1}. \tag{17}$$

The objective function in (15) can be decomposed into three easy-to-evaluate terms as [22]

$$\begin{aligned}&\|\mathbf{y}_1-\mathbf{B}\mathbf{p}_u-\mathbf{C}\mathbf{k}+\mathbf{b}\|^2_{\mathbf{W}_1}\\ =&\|\mathbf{y}_1-\mathbf{B}\hat{\mathbf{p}}_u-\mathbf{C}\hat{\mathbf{k}}+\mathbf{b}\|^2_{\mathbf{W}_1}+\|\hat{\mathbf{k}}-\mathbf{k}\|^2_{\mathbf{Q}^{-1}_{\hat{\mathbf{k}}}}+\|\hat{\mathbf{p}}_u(\mathbf{k})-\mathbf{p}_u\|^2_{\mathbf{Q}^{-1}_{\hat{\mathbf{p}}_u(\mathbf{k})}},\end{aligned} \tag{18}$$

where $\hat{\mathbf{p}}_u(\mathbf{k})$ represents the LS solution conditioned on $\mathbf{k}$. That is

$$\hat{\mathbf{p}}_u(\mathbf{k})=\hat{\mathbf{p}}_u-\mathbf{Q}_{\hat{\mathbf{k}}\hat{\mathbf{p}}_u}\mathbf{Q}^{-1}_{\hat{\mathbf{k}}}\left(\hat{\mathbf{k}}-\mathbf{k}\right), \tag{19}$$

and the corresponding covariance matrix is $\mathbf{Q}_{\hat{\mathbf{p}}_u(\mathbf{k})}=\mathbf{Q}_{\hat{\mathbf{p}}_u}-\mathbf{Q}_{\hat{\mathbf{p}}_u\hat{\mathbf{k}}}\mathbf{Q}^{-1}_{\hat{\mathbf{k}}}\mathbf{Q}_{\hat{\mathbf{k}}\hat{\mathbf{p}}_u}$. The first term on the right-hand side of (18) is given in a close-form. The last term of (18) is irrelevant to the integer search and can be eliminated [22]. Therefore, the optimization (15) reduces to

$$\check{\mathbf{k}}=\arg\min_{\mathbf{k}\in\mathbb{Z}^{N-1}}\|\hat{\mathbf{k}}-\mathbf{k}\|^2_{\mathbf{Q}^{-1}_{\hat{\mathbf{k}}}}, \tag{20}$$

The LAMBDA method is usually utilized to resolve the unknown integers in (20) because of its high computational efficiency and capacity to maximize the success rate [22]. Once the integer ambiguities are resolved, the updated receiver position is given by $\check{\mathbf{p}}_u=\hat{\mathbf{p}}_u\left(\check{\mathbf{k}}\right)$.

B. The Proposed Hybrid GNSS-5G Localization Algorithm

1) Initialization: Since (12) is a non-convex optimization problem, proper initialization is essential to avoid local minima. In general, one can consider using the float RTK solution in (16) as an initial user position and float carrier-phase ambiguities, and the clock bias can be randomly initialized from a uniform distribution as $\tilde{\Delta}_0\sim\mathcal{U}(0,T_c)$ with T_c is the clock cycle of the user, that is

$$\mathbf{x}_0=[\hat{\mathbf{p}}_u^\mathsf{T},\hat{\mathbf{k}}^\mathsf{T},\tilde{\Delta}_0]^\mathsf{T}. \tag{21}$$

However, the standalone RTK solution may not be available in some cases, as will be discussed in the next subsection. Under these circumstances, we can initialize based on the 5G observations using

$$\mathbf{x}_0=[\hat{\mathbf{p}}_{u,0}^\mathsf{T},\hat{\mathbf{k}}_0^\mathsf{T},\tilde{\Delta}_0]^\mathsf{T}. \tag{22}$$

Here, $\hat{\mathbf{p}}_{u,0}$ is estimated as

$$\hat{\mathbf{p}}_{u,0}=\frac{1}{L}\sum_{\ell=1}^{L}\left(\mathbf{p}_{\mathrm{B},\ell}+c\tau_\ell\mathbf{R}_{\mathrm{B},\ell}\mathbf{t}_\ell\right), \tag{23}$$

where $\mathbf{t}_\ell=\left[\cos(\theta^{\mathrm{az}}_\ell)\cos(\theta^{\mathrm{el}}_\ell),\sin(\theta^{\mathrm{az}}_\ell)\cos(\theta^{\mathrm{el}}_\ell),\sin(\theta^{\mathrm{el}}_\ell)\right]^\mathsf{T}$. The float carrier-phase ambiguities $\hat{\mathbf{k}}_0$ can be estimated based on the LS solution of (15) given $\mathbf{p}_u=\hat{\mathbf{p}}_{u,0}$, i.e.,

$$\hat{\mathbf{k}}_0=\left(\mathbf{C}^\mathsf{T}\mathbf{W}_1\mathbf{C}\right)^{-1}\mathbf{C}^\mathsf{T}\mathbf{W}_1\left(\mathbf{y}_1-\mathbf{B}\hat{\mathbf{p}}_{u,0}+\mathbf{b}\right). \tag{24}$$

2) Float Solution: With proper initialization, we can obtain a float solution of (12) by ignoring the integer constraint on $\mathbf{k}$. In this case the problem (12) is reduced to

$$\underset{\mathbf{x}\in\mathbb{R}^{N+3}}{\arg\min}\ \epsilon\|\hat{\mathbf{y}}_1-\mathbf{A}\mathbf{x}+\mathbf{b}\|^2_{\mathbf{W}_1}+(1-\epsilon)\|\hat{\mathbf{y}}_2-\mathbf{y}_2(\mathbf{x})\|^2_{\mathbf{W}_2}. \tag{25}$$

A gradient-based algorithm (such as gradient descent) can be applied to solve (25). We define $f_1\triangleq\|\hat{\mathbf{y}}_1-\mathbf{A}\mathbf{x}+\mathbf{b}\|^2_{\mathbf{W}_1}$ and $f_2\triangleq\|\hat{\mathbf{y}}_2-\mathbf{y}_2(\mathbf{x})\|^2_{\mathbf{W}_2}$. The first-order derivatives $\partial f_1/\partial\mathbf{x}$ and $\partial f_2/\partial\mathbf{x}$ for the iterative algorithm are given by

$$\partial f_1/\partial\mathbf{x}=-2\mathbf{A}^\mathsf{T}\mathbf{W}_1(\hat{\mathbf{y}}_1-\mathbf{A}\mathbf{x}+\mathbf{b}), \tag{26}$$

$$\partial f_2/\partial\mathbf{x}=-2\left(\frac{\partial\mathbf{y}_2(\mathbf{x})}{\partial\mathbf{x}}\right)^\mathsf{T}\mathbf{W}_2\left(\hat{\mathbf{y}}_2-\mathbf{y}_2(\mathbf{x})\right). \tag{27}$$

The expressions of $\partial\mathbf{y}_2(\mathbf{x})/\partial\mathbf{x}$ can be collected from the following derivatives:

$$\begin{aligned}&\partial\theta^{\mathrm{az}}_\ell/\partial\mathbf{p}_u=s_1\frac{(\mathbf{u}_1^\mathsf{T}\mathbf{t}_\ell)\mathbf{R}_{\mathrm{B},\ell}\mathbf{u}_2-(\mathbf{u}_2^\mathsf{T}\mathbf{t}_\ell)\mathbf{R}_{\mathrm{B},\ell}\mathbf{u}_1}{(\mathbf{u}_1^\mathsf{T}\mathbf{t}_\ell)^2},\\ &\partial\theta^{\mathrm{el}}_\ell/\partial\mathbf{p}_u=s_2\left(\frac{\mathbf{R}_{\mathrm{B},\ell}\mathbf{u}_3}{d_\ell}-\frac{(\mathbf{u}_3^\mathsf{T}\mathbf{t}_\ell)(\mathbf{p}_u-\mathbf{p}_{\mathrm{B},\ell})}{d_\ell^3}\right),\\ &\partial\tau_\ell/\partial\mathbf{p}_u=\frac{\mathbf{p}_u-\mathbf{p}_{\mathrm{B},\ell}}{cd_\ell},\quad\frac{\partial\tau_\ell}{\partial\Delta}=1,\end{aligned}$$

where

$$\begin{aligned}&\mathbf{u}_1=[1,0,0]^\mathsf{T},\ \mathbf{u}_2=[0,1,0]^\mathsf{T},\ \mathbf{u}_3=[0,0,1]^\mathsf{T},\\ &d_\ell=\|\mathbf{p}_u-\mathbf{p}_{\mathrm{B},\ell}\|_2,\quad\mathbf{t}_\ell=\mathbf{R}^\mathsf{T}_{\mathrm{B},\ell}(\mathbf{p}_u-\mathbf{p}_{\mathrm{B},\ell}),\\ &s_1=\left[1+\left(\frac{\mathbf{u}_2^\mathsf{T}\mathbf{t}_\ell}{\mathbf{u}_1^\mathsf{T}\mathbf{t}_\ell}\right)^2\right]^{-1},\ s_2=\left[1-\left(\frac{\mathbf{u}_3^\mathsf{T}\mathbf{t}_\ell}{d_\ell}\right)^2\right]^{-\frac{1}{2}}.\end{aligned}$$

3) Ambiguity Resolution: Suppose a float solution $\hat{\mathbf{x}}=[\hat{\mathbf{p}}_u^\mathsf{T},\hat{\mathbf{k}}^\mathsf{T},\hat{\Delta}]^\mathsf{T}$ is obtained by solving (25). The integer carrier-phase ambiguity resolution step can be achieved by the same routine as Subsection III-A, i.e., solving (20) using, e.g., the LAMBDA methods. Therefore, the integer ambiguity estimate is obtained as $\check{\mathbf{k}}$.

TABLE I
DEMONSTRATION OF THE LOCALIZATION AVAILABILITY.*

(n_o, n_u) / L \ N	0	1	2	3	4	5
0	~~(0, 3)~~	~~(0, 3)~~	~~(2, 4)~~	~~(4, 5)~~	(6, 6)	(8, 7)
1	~~(3, 4)~~	~~(3, 4)~~	(5, 5)	(7, 6)	(9, 7)	(11, 8)

* Here n_o and n_u represent the number of observations and unknowns, respectively. The nonlocalizable cases ($n_o < n_u$) are marked by a strikethrough.

4) Fixed Solution: After the ambiguity resolution, the fixed solution can be obtained through the following optimization:

$$\underset{\mathbf{p}_u \in \mathbb{R}^3, \Delta \in \mathbb{R}}{\arg\min} \quad \epsilon \|\hat{\mathbf{y}}_1 - \mathbf{A}\mathbf{x} + \mathbf{b}\|^2_{\mathbf{W}_1} + (1-\epsilon)\|\hat{\mathbf{y}}_2 - \mathbf{y}_2(\mathbf{x})\|^2_{\mathbf{W}_2}, \quad (28)$$

with a fixed $\mathbf{k} = \check{\mathbf{k}}$. The solution is returned as $\check{\mathbf{p}}_u$ and $\check{\Delta}$. Finally, we have the joint estimate as $\check{\mathbf{x}} = [\check{\mathbf{p}}_u^\mathsf{T}, \check{\mathbf{k}}^\mathsf{T}, \check{\Delta}]^\mathsf{T}$.

C. Localization Availability Analysis

Generally, the RTK technique requires at least 4 satellites to perform localization. However, by incorporating the 5G observations, this constraint can be further relaxed. The localization availability can be determined by comparing the dimensionality of the observations and that of the unknowns. In general, the number of observations should be equal to or greater than the number of unknowns to make the estimation problem solvable with a unique solution. In this paper, we name the cases with the localization uniqueness (i.e., the observations' dimension is not less than unknowns) as the *localizable* cases, otherwise *nonlocalizable* cases. Taking the case where $N = 3$ and $L = 1$ as an example, we can check the unknown $\mathbf{x} \in \mathbb{R}^6$ in (11) and the observations $[\mathbf{y}_1^\mathsf{T}, \mathbf{y}_2^\mathsf{T}]^\mathsf{T} \in \mathbb{R}^7$ in (6) and (10). As the dimension of the observations is higher than the unknowns, the user is localizable when $N = 3$ and $L = 1$. A summary of the localization availability in different scenarios is presented in Table I. We can see that leveraging 5G observations enhances the localization availability. For example, with a single 5G BS, localization is available in the cases of $N = 2$ and $N = 3$. Note that having 5G observations from two or more BSs is sufficient to perform localization regardless of GNSS availability.

IV. PERFORMANCE EVALUATION

A. Simulation Setup

The simulations are implemented using the actual satellite orbit information in the GPS Yuma Almanacs file on January 01, 2023. The positions and the orientations of the 5G BSs are generated randomly within a $50\,\mathrm{m} \times 50\,\mathrm{m} \times 50\,\mathrm{m}$ space. We assume the observations $\mathbf{y}_1 = [\mathbf{p}^\mathsf{T}, \boldsymbol{\phi}^\mathsf{T}]^\mathsf{T}$ and $\mathbf{y}_2$ to be contaminated with zero-mean additive Gaussian noises controlled by their standard deviations. We set the standard deviation of the carrier-phase measurements equal to a value σ and that of the pseudo-range data equal to 100σ. The standard deviation of the noise of $\mathbf{y}_2$ is fixed based on the Fisher information matrix of the 5G channel estimation step, as detailed in, e.g., [23]–[25].

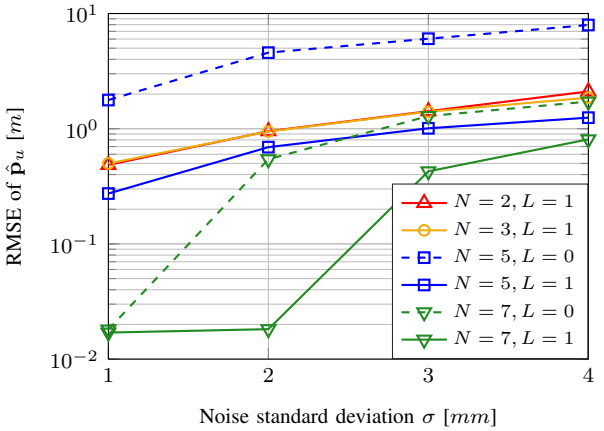

Fig. 2. Evaluation of positioning RMSE versus the noise standard deviation of the carrier-phase noise for different numbers of satellites N and $L = \{1, 0\}$.

In the cases where $L = 0$, the results are obtained from the ILS solution in Subsection III-A. In all other cases, the proposed method developed in Subsection III-B is used with a weighting factor $\epsilon = 0.6$. The iterative procedure for solving (12) is implemented using the Manopt toolbox [26]. All the involved root mean square errors (RMSEs) are computed through 500 Monte Carlo simulations.

B. Results Analysis

Fig. 2 presents the RMSE of estimated $\hat{\mathbf{p}}_u$ versus the noise standard deviation σ for different number of satellites N and fixed $L = \{1, 0\}$. In general, we can see that the RMSE increases as the noise level increases. By comparing the cases of $L = 0$ (dashed curves) and $L = 1$ (solid curves) for the same N, we observe that adding one 5G BS offers a significant reduction in estimation error, demonstrating that the utilization of the 5G observations can provide a remarkable improvement in localization performance. Moreover, it is noted that with the 5G observations involved, localization in the cases where $N = 2$ and $N = 3$ become not only localizable but also with higher accuracy than the case with 5-satellite and no 5G aid (dashed blue curve). In addition, by comparing the cases of different N with the same L, we observe that the more satellites available, the lower the estimation error is. It is also noted that the performance of the cases $N = 2$ and $N = 3$ is very close, indicating that with insufficient satellites ($N < 4$), the location information is mainly derived from the 5G observations and changing the number of satellite within $N < 4$ cannot boost performance significantly.

Fig. 3 plots the RMSE of $\hat{\mathbf{p}}_u$ versus the carrier-phase noise standard deviation σ for different numbers of 5G BSs L and fixed $N = \{5, 7\}$. The results show that for the same number of satellites, the more 5G BSs we deploy, the better localization performance we obtain, especially for $L \in \{0, 1, 2\}$. However, when more than two 5G BSs are available, continuing to increase the number of 5G BSs may not significantly improve performance.

Finally, we evaluate the success rate of carrier-phase ambiguity resolution, an important performance indicator for

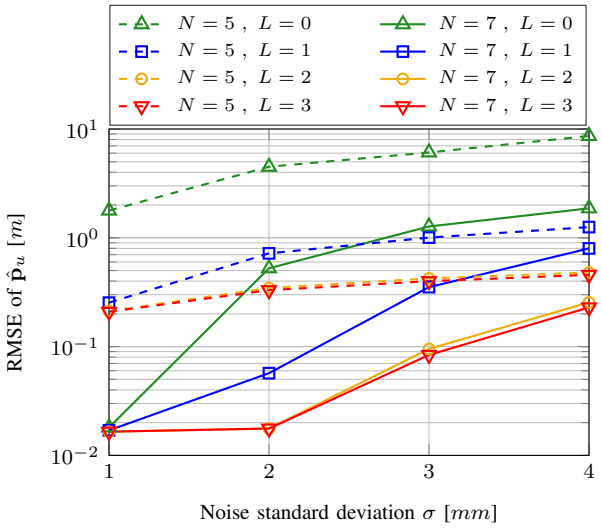

Fig. 3. Positioning RMSE versus carrier-phase noise standard deviation for different numbers of 5G BS $L \in \{0, 1, 2, 3\}$ and different numbers of satellites $N \in \{5, 7\}$).

TABLE II
SUCCESS RATE OF THE CARRIER-PHASE AMBIGUITY RESOLUTION

L \ N	2	3	4	5	6	7
0	0.00 %	0.00 %	7.02 %	54.39 %	94.66 %	99.99 %
1	36.08 %	45.17 %	51.24 %	73.58 %	99.06 %	100.00 %

GNSS-based positioning. Performance is computed from 10000 Monte Carlo trials for each case. The results are shown in Table II. It is clearly visible that the introduction of 5G observations can increase the ambiguity resolution success rate. Additionally, in general, access to more satellite observations is also helpful.

V. CONCLUSION

This paper formulated, analyzed, and solved a 5G-aided GNSS localization problem in satellite-deprived environments. A novel gradient-based algorithm, coupled with a proposed ambiguity resolution method, is applied to estimate the user's location using GNSS and 5G observations simultaneously. The presented results reveal that the proposed approach enhances localization accuracy and GNSS ambiguity resolution success rates, especially in scenarios with extremely limited satellite visibility.

ACKNOWLEDGEMENT

This publication is based upon work supported by the King Abdullah University of Science and Technology (KAUST) Office of Sponsored Research (OSR) under Award No. ORA-CRG2021-4695.

REFERENCES

[1] D. Fernandez-Llorca, R. Quintero Minguez *et al.*, "Assistive intelligent transportation systems: The need for user localization and anonymous disability identification," *IEEE Intelligent Transportation Systems Magazine*, vol. 9, no. 2, pp. 25–40, 2017.

[2] S. J. LeVoir, P. A. Farley *et al.*, "High-accuracy adaptive low-cost location sensing subsystems for autonomous rover in precision agriculture," *IEEE Open Journal of Industry Applications*, vol. 1, pp. 74–94, 2020.

[3] M. Usman, M. R. Asghar *et al.*, "Technologies and solutions for location-based services in smart cities: Past, present, and future," *IEEE Access*, vol. 6, pp. 22 240–22 248, 2018.

[4] S. Yuan, H. Wang *et al.*, "Survey on localization systems and algorithms for unmanned systems," *Unmanned Systems*, vol. 9, no. 02, pp. 129–163, 2021.

[5] B. M. Chen, "On the trends of autonomous unmanned systems research," *Engineering*, vol. 12, pp. 20–23, 2021.

[6] C. Jeffrey, *An introduction to GNSS: GPS, GLONASS, Galileo and other global navigation satellite systems*. NovAtel, 2010.

[7] A. Parkins, "Increasing GNSS RTK availability with a new single-epoch batch partial ambiguity resolution algorithm," *GPS solutions*, vol. 15, no. 4, pp. 391–402, 2011.

[8] B. Hofmann-Wellenhof, H. Lichtenegger *et al.*, *GNSS–Global Navigation Satellite Systems: GPS, GLONASS, Galileo, and more*. Springer Science & Business Media, 2007.

[9] X. Liu, T. Ballal *et al.*, "GNSS-based localization for autonomous vehicles: Prospects and challenges," in *Proc. 27th Eur. Signal Process. Conf.(EUSIPCO)*, 2019, pp. 2–6.

[10] T. Li, H. Zhang *et al.*, "High-accuracy positioning in urban environments using single-frequency multi-GNSS RTK/MEMS-IMU integration," *Remote sensing*, vol. 10, no. 2, p. 205, 2018.

[11] A. Schütz, D. E. Sánchez-Morales *et al.*, "Precise positioning through a loosely-coupled sensor fusion of GNSS-RTK, INS and LiDAR for autonomous driving," in *2020 IEEE/ION Position, Location and Navigation Symposium (PLANS)*. IEEE, 2020, pp. 219–225.

[12] M. Koivisto, A. Hakkarainen *et al.*, "High-efficiency device positioning and location-aware communications in dense 5G networks," *IEEE Communications Magazine*, vol. 55, no. 8, pp. 188–195, 2017.

[13] M. Koivisto, M. Costa *et al.*, "Joint device positioning and clock synchronization in 5G ultra-dense networks," *IEEE Transactions on Wireless Communications*, vol. 16, no. 5, pp. 2866–2881, 2017.

[14] A. Shahmansoori, G. E. Garcia *et al.*, "Position and orientation estimation through millimeter-wave MIMO in 5G systems," *IEEE Transactions on Wireless Communications*, vol. 17, no. 3, pp. 1822–1835, 2018.

[15] C. De Lima, D. Belot *et al.*, "Convergent communication, sensing and localization in 6G systems: An overview of technologies, opportunities and challenges," *IEEE Access*, vol. 9, pp. 26 902–26 925, 2021.

[16] L. Yin, Q. Ni *et al.*, "A GNSS/5G integrated positioning methodology in D2D communication networks," *IEEE Journal on Selected Areas in Communications*, vol. 36, no. 2, pp. 351–362, 2018.

[17] R. Klus, J. Talvitie *et al.*, "Neural network fingerprinting and GNSS data fusion for improved localization in 5G," in *2021 International Conference on Localization and GNSS (ICL-GNSS)*, 2021, pp. 1–6.

[18] L. Bai, C. Sun *et al.*, "GNSS-5G hybrid positioning based on multi-rate measurements fusion and proactive measurement uncertainty prediction," *IEEE Transactions on Instrumentation and Measurement*, vol. 71, pp. 1–15, 2022.

[19] G. Destino, J. Saloranta *et al.*, "Performance analysis of hybrid 5G-GNSS localization," in *2018 52nd Asilomar Conference on Signals, Systems, and Computers*, 2018, pp. 8–12.

[20] A. Minetto, M. C. Bello *et al.*, "DGNSS cooperative positioning in mobile smart devices: A proof of concept," *IEEE Transactions on Vehicular Technology*, vol. 71, no. 4, pp. 3480–3494, 2022.

[21] P. J. Teunissen and O. Montenbruck, *Springer handbook of global navigation satellite systems*. Springer, 2017, vol. 10.

[22] P. Teunnissen, "The least-square ambiguity decorrelation adjustment: a method for fast GPS integer ambiguity estimation," *J. Geodesy*, vol. 70, no. 1, pp. 65–82, 1995.

[23] P. Zheng, H. Chen *et al.*, "Misspecified Cramér-Rao bound of RIS-aided localization under geometry mismatch," *IEEE ICASSP*, 2023.

[24] H. Chen, H. Sarieddeen *et al.*, "A tutorial on terahertz-band localization for 6G communication systems," *IEEE Communications Surveys & Tutorials*, vol. 24, no. 3, pp. 1780–1815, 2022.

[25] P. Zheng, T. Ballal *et al.*, "Coverage analysis of joint localization and communication in THz systems with 3D arrays," *TechRxiv preprint*, 2022.

[26] N. Boumal, B. Mishra *et al.*, "Manopt, a Matlab toolbox for optimization on manifolds," *Journal of Machine Learning Research*, vol. 15, no. 42, pp. 1455–1459, 2014. [Online]. Available: https://www.manopt.org